Nuclear track detectors in particle, astroparticle and nuclear physics

L. Patrizii[a] and Z. Sahnoun[a,b]
[a] *INFN, Sez. Bologna, 40127 Bologna, Italy.*
[b] *Astrophysics Dept., CRAAG, 16340 Algiers, Algeria.*

Recibido el 11 de marzo de 2009; aceptado el 11 de agosto de 2009

Applications of nuclear track detectors in particle, astroparticle and nuclear physics are discussed. The main focus concerns the searches for point-like magnetic monopoles at accelerators and in the cosmic radiation. Results of the measurements of fragmentation cross-sections in relativistic heavy ion collisions are also presented.

Keywords: Nuclear track detectors; astroparticle; nuclear physics.

En este trabajo se discuten las aplicaciones de los detectores de trazas, en las áreas de Física de partículas, Astropartículas y Física Nuclear. El objetivo principal consiste en la búsqueda de monopolos magnéticos de tipo puntual en aceleradores y en la radiación cósmica. También son presentados los resultados de las medidas de fragmentación en colisiones de iones pesados relativísticos.

Descriptores: Detectores por trazas nucleares; astropartículas; física nuclear.

PACS: 14.80.Hv-j; 21.65.-f; 29.40.Wk; 29.90.+r

1. Introduction

Nuclear track detectors (NTDs) have long been successfully applied in various fields

At accelerators, by exploiting their resistance to radiation and the excellent charge resolution, NTDs allow searches for the production of heavy ionizing particles, such as point-like magnetic monopoles and studies of heavy ions fragmentation processes. In many cases, when the event flu is expected to be small, as in searches for exotic particles in the cosmic radiation, NTDs being passive, low cost, reliable on a long run and easy to deploy represent a viable detection technique.

In this paper, after recalling the calibration procedure of NTDs used in the applications discussed here, we report about the latest results on:

i) searches for point-like magnetic monopoles at accelerators;

ii) the measurement of the fragmentation cross sections of fast heavy ions;

iii) the search in the cosmic radiation (CR) for massive penetrating particles.

2. NTDs: working mechanism and calibration procedure

"Track-etch" detectors are able to record the passage of heavily ionizing particles which leave in the material a damage zone ("latent track") of $\sim$10 nm diameter along their trajectory. The latent track can be amplifie and, by applying a proper chemical etching, it appears as a cone shaped etch-pit [1]. For plastic materials typical etching solutions are sodium hydroxide (NaOH) solutions at high concentration (6N,8N) and temperatures (70°C, 80°C). The depth of the etch-pit is an increasing function of Z/β, where Z is the charge of the particle and β =v/c is the particle velocity relative to the speed of light. A schematic of NTDs' working mechanism is shown in Fig. 1.

In plastics, such as CR39®, the formation of an etchable track can be related to the Restricted Energy Loss (REL) of the passing particle, which is the energy lost in a cylindrical region of about 10 nm diameter around the particle trajectory. The response of track-etch detectors versus REL can be established by a proper calibration using ions of different charges and energies. For searches discussed in this paper a typical calibration set-up consists of stacked NTD foils upstream and downstream of a target exposed at accelerators to high energy heavy ion beams (Fig. 2). The main advantage of this set-up is that downstream detector foils can detect both beam ions and their fragments produced (mainly) in the target; in this way with a single exposure one can calibrate the detector over a wide energy loss interval.

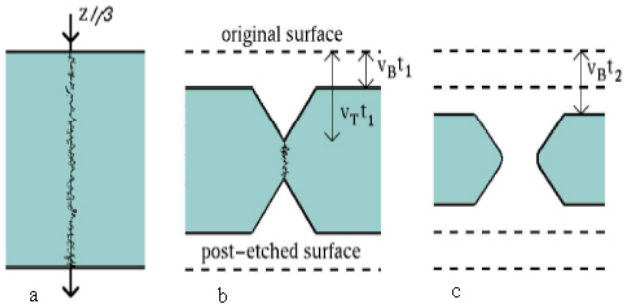

FIGURE 1. Schematic of the working mechanism of "track-etch" detectors. **a)** a charged particle crossing the detector creates along its path a damaged zone ("latent track"); **b)** chemical etching results in the formation of "etch-pit" cones on each side of the detector since material along the latent track is etched out at a rate v_T larger than the bulk etching rate v_B; **c)** etch-pit cones link after a prolonged etching.

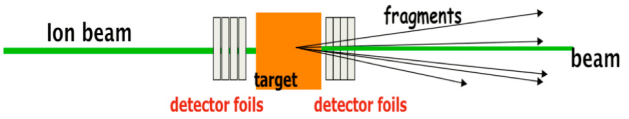

FIGURE 2. A sketch of a calibration set-up with a beam at an ion accelerator.

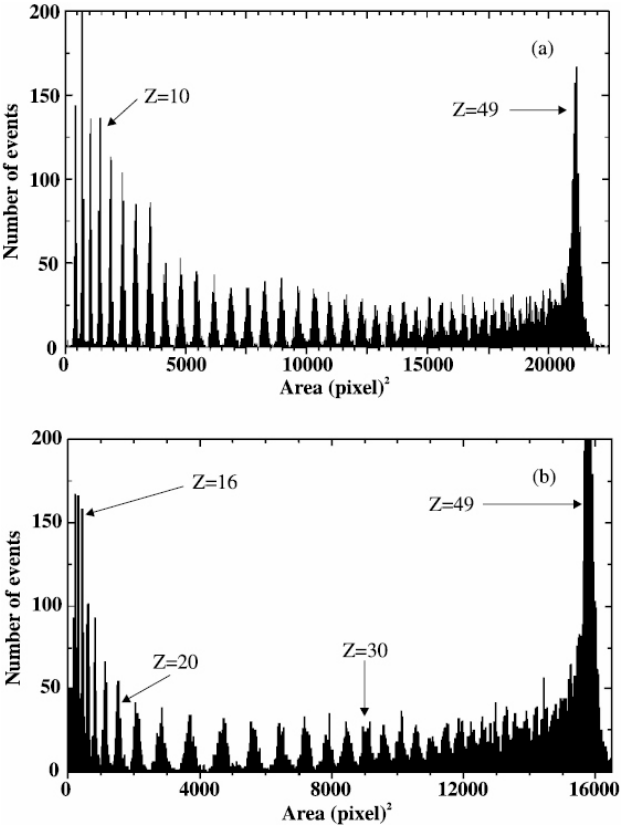

FIGURE 3. Distribution of the base areas of etch-pit cones in CR39®from relativistic In^{49+} ions and their fragments. The base areas were averaged over two measurements (two detector foils). The CR39®was etched in **(a)** soft and **(b)** strong etching conditions.

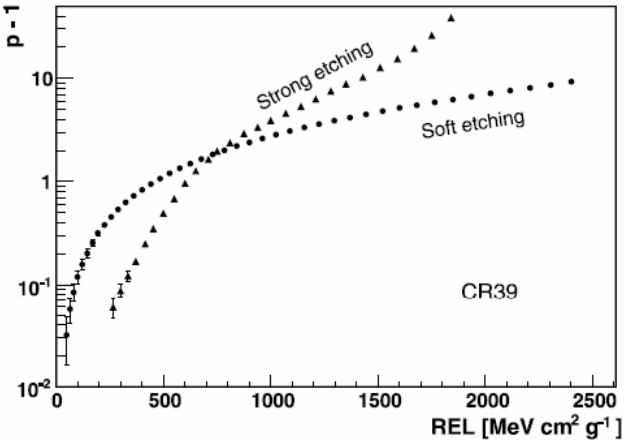

FIGURE 4. Reduced etch-rate p-1 vs. REL for CR39®etched in soft and strong conditions.

In Fig. 3 is shown, as an example, the distribution in CR39®of the base areas of etch-pit cones produced by 158 AGeV In^{49+} ions at the CERN SPS and by their fragments. After exposure to the ion beam the CR39®foils were etched in 6N NaOH + 1% ethyl alcohol at 70°C ("soft" etching, Fig. 3a) and in 8N KOH + 1.5% ethyl alcohol at 75°C ("strong" etching, Fig. 3b). Each peak corresponds to an ion fragment of decreasing charge starting at the highest peak which corresponds to the ion beam. For each recorded charged fragment the REL can be computed; from the area distribution the reduced etch rate p= $v_T/v_B{}^i$ is determined. The calibration data are given by the reduced etch-rate p vs. REL, as shown in Fig. 4. The detection thresholds are at REL∼50 and 250 MeVcm^2 g^{-1} for CR39®etched in the soft and strong etching condition, respectively [2-4].

3. "Dirac" magnetic monopoles

In 1931 P.A.M. Dirac introduced the concept of the magnetic monopole (MM) in order to explain the quantization of the electric charge e [5]. He established the relationship $eg = n\eta c/2$ where n is an integer, n= 1, 2, 3, ..., from which the magnetic charge g= ng_D; $g_D = \eta c/2e$= 68.5e, is called the unit Dirac charge. The existence of magnetic charges and of magnetic currents would symmetrize in form Maxwell's equations, but the symmetry would not be perfect since $e \ll g$. There is no real prediction for the mass of classical "Dirac" monopole. A rough estimate was made assuming that the classical monopole radius is equal to the classical electron radius, $r_M = g^2/(m_M c^2) = r_e = e^2/m_e c^2$ from which $m_M = g^2 m_e/e^2 \approx n{\cdot}4700{\cdot}m_e = n{\cdot}2.4$ GeV/c^2. Thus the MM mass should be relatively large and even larger if the basic electric charge is that of quarks, e/3, and if $n > 1$.

The main properties of magnetic monopoles are obtained from the Dirac relation and the most important ones are recalled here.

- *Basic magnetic charge.* If n =1 and the basic electric charge is that of the electron, then the magnetic charge, $g_D = \eta c/2e = 137e/2$, in general, $g = ng_D$.
- *Electric charge*. Electrically charged monopoles (dyons) may arise as quantum mechanical excitations or as M-p, M-nucleus composites.
- *Dimensionless magnetic coupling constant.* In analogy with the fin structure constant, $\alpha = e^2/\eta c \approx 1/137$, the dimensionless coupling constant is define as $\alpha_g = g_D^2/\eta c \approx 34.25$. As it is greater than one, perturbative calculations cannot be used.
- *Spin.* The spin of the magnetic monopole is usually taken to be 1/2 or 0.
- *Energy W acquired in a magnetic field B.* W = ng_DB $l = n$ 20.5 keV/G.cm. In a coherent galactic length ($l <$ 1 kpc, B ≈ 3μG), the energy gained by a magnetic

monopole with $g{=}g_D$ is W $\sim 1.8{\times}10^{11}$ GeV. Classical poles and intermediate mass magnetic monopoles in cosmic rays may be accelerated to relativistic velocities. GUT poles should have low velocities, $10^{-4} < \beta < 10^{-1}$.

- *Trapping.* Magnetic monopoles may be trapped in ferromagnetic materials by an image force, which could reach values of < 10 eV/Å.

3.1. Energy losses of magnetic monopoles

A relativistic monopole with magnetic charge g_D and velocity v = βc behaves like an equivalent electric charge $(Ze)_{eq}{=}g_D\beta$; the energy losses of fast monopoles are thus very large. In fact, the ionization caused by a relativistic monopole is $\sim$ 4700 times that of a minimum ionizing particle [6]. Unlike electrically charged particles, dE/dx should *decrease* for a monopole passing through a detector. Electronic energy loss (*i.e.* the energy lost in ionization or excitation of atoms and molecules of the medium) predominates for electrically or magnetically charged particles with $\beta > 10^{-3}$; the dE/dx of magnetic monopoles with $10^{-4} < \beta < 10^{-3}$ is mainly due to excitations of atoms and molecules of the medium. At very low velocities, $\beta < 10^{-4}$, magnetic monopoles cannot excite atoms; they can only lose energy in elastic collisions with atoms or with nuclei. The energy is released to the medium in the form of elastic vibrations and/or infra–red radiation.

In Fig. 5 are shown the restricted energy losses in CR39®NTDs of MMs with magnetic charges g_D, $2g_D$ and $3g_D$ versus their velocity β [7]. Both the electronic and the nuclear energy losses contribute to REL. It was shown that both are effective in producing etchable tracks in a CR39®nuclear track detector [8].

3.2. MM searches at accelerators using NTDs

Since 1931 searches for classical ("Dirac") monopoles were carried out at every new accelerator using mainly relatively simple experiments, and recently also at large collider detectors [9-11]. In more than 15 of such experiments NTDs were used. The experimental set-up is very simple. It usually consists of multi layered stacks of NTDs surrounding the intersection region. After exposure, the detectors are etched; the front-most layer (with respect to the intersection point) is scanned using low magnificatio optical microscopes; by relying on special marker holes, it is possible to determine the position of candidate events with an accuracy better than $\sim$20 μm.

CR39®NTD can have a threshold as low as Z/$\beta \approx 5$; it is the most sensitive detector and it allows to search for magnetic monopoles with one unit Dirac charge ($g = g_D$) for β around 10^{-4}, for $\beta > 10^{-3}$ and the whole β-range of $4{\times}10^{-5} < \beta < 1$ for magnetic monopoles with $g \geq 2g_D$ [12]. Lexan and Makrofol polycarbonates having a threshold at Z/$\beta \approx 50$ are sensitive only to relativistic magnetic monopoles.

The firs search experiment to use NTDs [6] was performed in 1975 at CERN; 12 stacks of Makrofol and nitrocellulose NTDs were placed around the intersection region I1 at the ISR. The exposure was made at $\sqrt{s}$ = 45 and 53.2 GeV and also at 62.8 GeV. A more recent search was performed

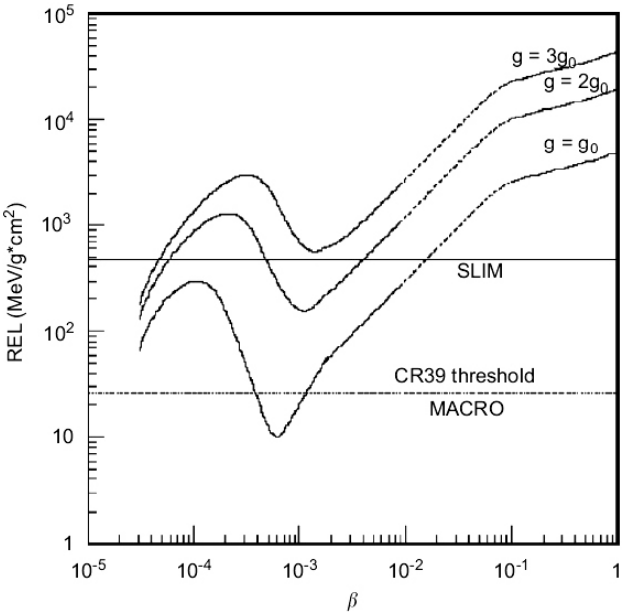

FIGURE 5. REL vs. β=v/c for MMs with magnetic charge $g{=}$ g_D, $2g_D$ and $3g_D$. Horizontal lines indicate the threshold of the CR39®used in the MACRO and SLIM experiments.

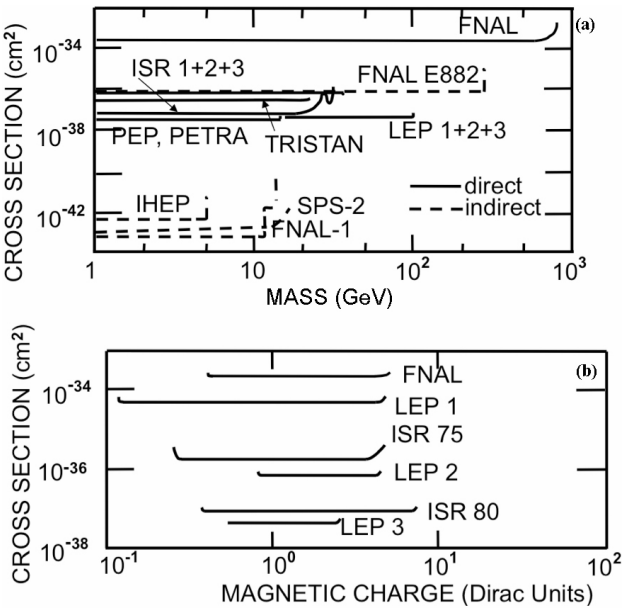

FIGURE 6. (a) Classical MMs cross section upper limits vs MM mass obtained from direct accelerator searches (solid lines) and indirect searches (dashed lines) [10,11,13-15]. (b) Upper limits on classical MMs production cross sections set by different experiments at accelerators, versus MM charge.

at the LEP e^+e^- collider, at CERN. The MODAL experiment [13] was run at $\sqrt{s}$ = 91.1 GeV energy. The mechanism for magnetic monopole production assumed annihilation and pair production via the electromagnetic interaction. The apparatus consisted in polyhedral array fille with stacks of CR39®plastic foils; it covered a 0.86 × 4π sr angle at the I5 interaction point at LEP. The integrated luminosity accumulated at $\sqrt{s}$ = 91.1 GeV was 60±12 nb^{-1}. The detector response was calibrated using heavy ions at the Lawrence Berkeley Laboratory. The general detection efficien y, assuming isotropic magnetic monopole pair production was simulated for charges g_D and $2g_D$.

No magnetic monopole was found in searches performed so far. In Fig. 6 are summarized the cross section upper limits (a) versus MM mass, and (b) versus the magnetic charge, set by various searches performed at accelerators (Ref. 9 and Refs. therein,10,11,13-15).

A future proposed experiment, MoEDAL [16], aims to use NTDs to search for magnetic monopoles at the CERN LHC accelerator complex. The LHC will operate at $\sqrt{s}$=14 TeV in the proton-proton mode. The MoEDAL experiment will cover a surface of ∼25 m^2 in the open intersection region of the LHCb experiment at point 8 on the LHC ring. If approved MoEDAL is due to start taking data with a limited deployment of detectors in 2009 and a full deployment of detectors in 2010. It will run in pp mode at a luminosity of 10^{32} cm^{-2} s^{-1} which is the highest available luminosity at point 8. The MoEDAL detector is designed to detect up to a ∼ 7 TeV mass monopole. MoEDAL will also have good sensitivity to multiply charged magnetic monopoles with g_D as high as 4.

4. Fragmentation cross-sections of heavy ions

Fragmentation studies of high energy ions are relevant for nuclear physics, cosmic ray physics, astrophysics and applied physics. Important applications of the propagation of fast heavy ion beams through matter are given in space radiation protection and in the fiel of cancer therapy. In Ref. 17 experimental results on the fragmentation of 158AGeV Pb^{82+} were reported.

New measurements of cross sections of charge changing fragmentation processes in the energy range 0.3 ÷ 10 A GeV of Fe^{26+} and Si^{14+} beams on polyethylene, CR39®and aluminum targets were reported in ref. [18]. The exposures were made at BNL, USA. Stacks composed of CR39®foils located upstream and downstream of the target were exposed to the ion beams at normal incidence (Fig.2). The target thickness was chosen as to optimize the fragmentation process. Charged fragments produced by projectile interactions with target nuclei keep most of the projectile longitudinal velocity. They can be detected after the target and followed through the stack. After exposures the CR39®foils were etched in 6N NaOH aqueous solution at 70°C for 30 h. An automatic image analyser system was used to scan the detector surfaces and measure the etch-pit cone base areas. A tracking procedure was used to reconstruct the path of the beam and of the fragments. The numbers N_i and N_s of beam ions before and after the target, respectively, were determined. The total fragmentation charge-changing cross-section for beam ions was evaluated from $\sigma_{tot} = X_T \cdot \ln(N_i/N_s)$, where $X_T = A_T/\rho_T \cdot t_T \cdot N_A$; ρ_T is the target density, A_T and t_T are the target atomic mass and thickness, respectively, and N_A is the Avogadro number. Multiple fragmentations in the target and in the detector foils were neglected. In Figs. 7 and 8 are shown the total cross section values versus energy for the silicon and iron beams, respectively, in Al, $(CH_2)_n$ and CR39®targets.

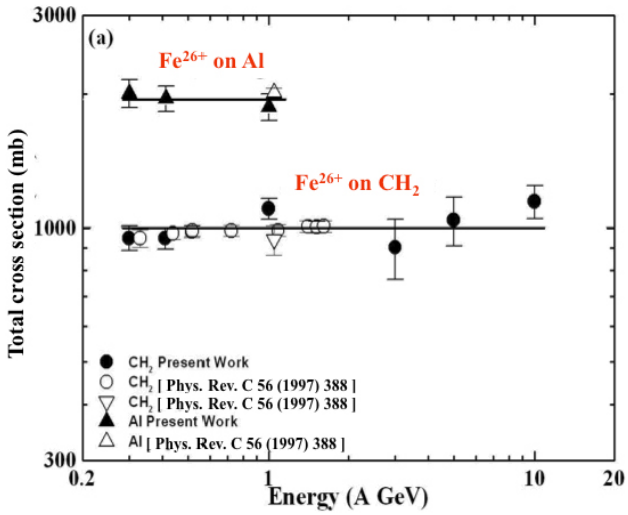

FIGURE 7. Total fragmentation cross sections for Fe^{26+} ions of different energies in CH_2 and Al targets.

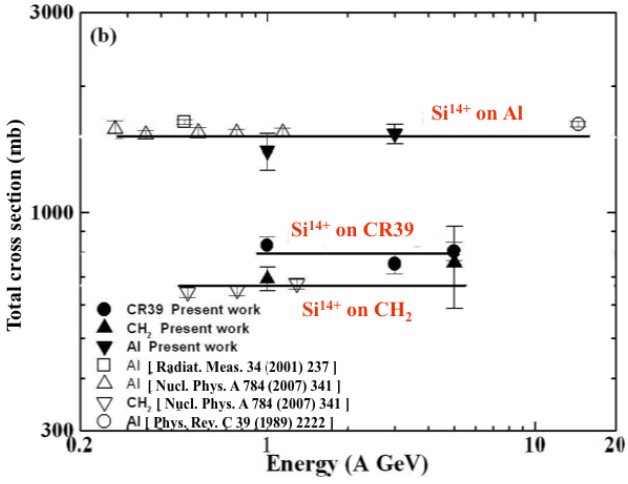

FIGURE 8. Total fragmentation cross sections for Si^{14+} ions in CH_2, CR39®and Al targets. The measured cross sections from other refs. and predictions are shown for comparison.

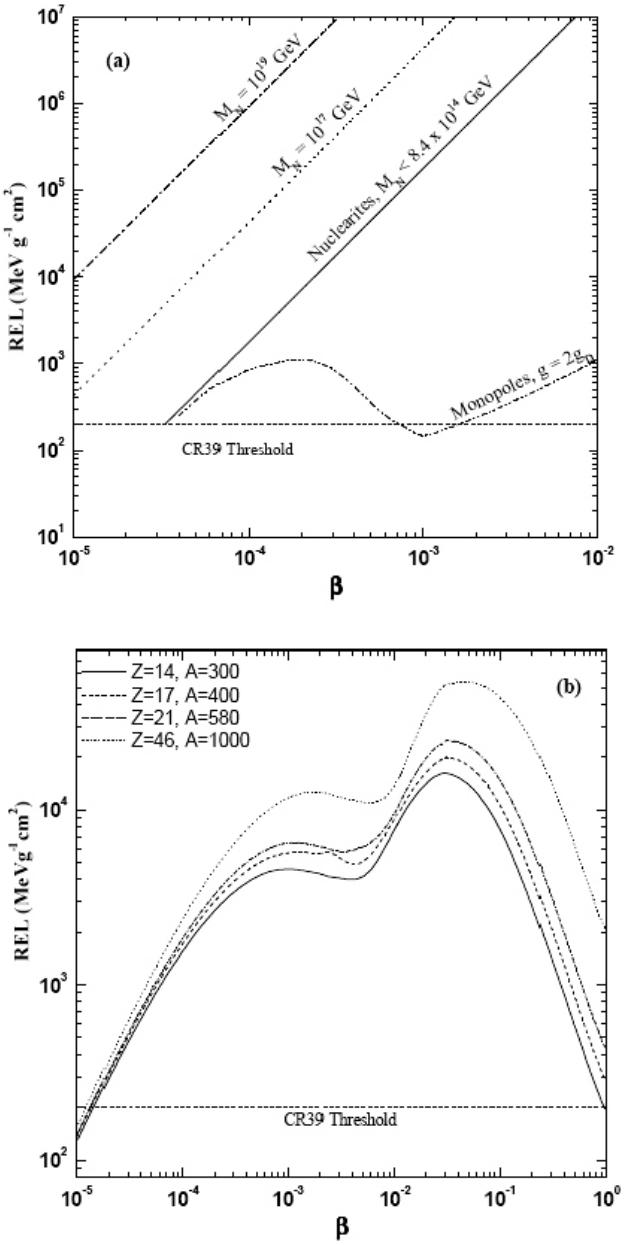

FIGURE 9. (a)REL versus β for nuclearites of different masses. The REL of magnetic monopoles with charge $g = 2g_D$ is also shown for comparison. (b) REL versus β for strangelets with different charges and masses. The strong etching threshold for CR39® is indicated by the horizontal line.

5. Search for exotica in the cosmic radiation

Nuclear track detectors (NTDs) are successfully applied in searches for particles incident (or hypothetically incident) on the Earth atmosphere such as supermassive and intermediate mass MMs and for lumps of strange quark matter (SQM).

GUT theories of electroweak and strong interactions predict the existence of MMs with masses of the order 10^{16}–10^{17}GeV. The MMs would appear in the Early Universe at the phase transition corresponding to the breaking of the GUT group into subgroups, one of which is U(1) [19,20]. Intermediate mass monopoles (IMMs) with $m_M \sim 10^5$– 10^{12}GeV may have been produced in later phase transitions in the Early Universe, when a semi-simple gauge group yields a U(1) group [21]. The lowest mass MM is stable, since magnetic charge is conserved like electric charge. Thus the poles produced in the Early Universe should still exist as cosmic relics in the cosmic radiation. A flu of cosmic GUT MMs may reach the Earth with a velocity spectrum in the range $4\times10^{-5} < \beta < 0.1$ peaked at $\beta \sim 10^{-3}$. IMMs may be accelerated up to relativistic velocities in one coherent galactic magnetic fiel domain. GUT poles have been searched for underground and IMMs at high altitude laboratories.

Similarly interesting are other particles such as Strange Quark Matter (SQM) lumps that can be constituents of the dark matter component of the Universe and possibly be present in the cosmic radiation [22]. Strange quark matter was introduced as the ground state of nuclear matter; it should consist of aggregates of u, $d$and $s$quarks in almost equal proportions [23]. The overall neutrality of SQM is ensured by an electron cloud that surrounds it, forming a sort of atom. SQM should have a constant density, slightly larger than that of atomic nuclei, and it should be stable for all baryon numbers in the range between ordinary heavy nuclei and neutron stars ($A \sim 10^{57}$). SQM could have been produced shortly after the Big Bang and may have survived as remnants; it could also appear in violent astrophysical processes, such as neutron/strange star collisions. Large lumps of SQM hypothetically present in the cosmic radiation are generally called "nuclearites". They should have typical galactic velocities, $\beta \sim 10^{-3}$, and for masses larger than 0.1 g could traverse the earth. Smaller SQM bags (A< 10^6 - 10^7) are often called "strangelets" and are expected to undergo the same acceleration and interaction processes as ordinary cosmic rays. Relativistic strangelets can only be searched for with experiments at very high altitude.

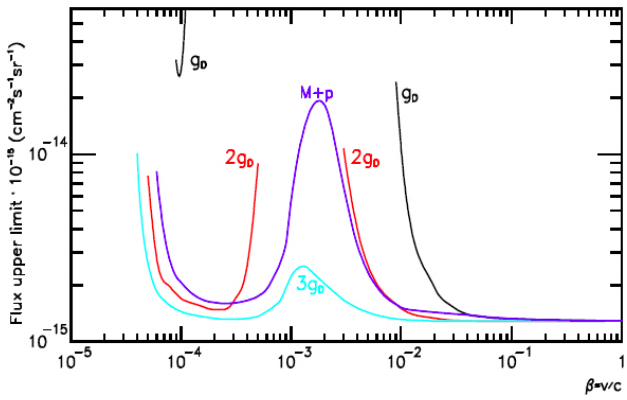

FIGURE 10. 90% C.L. upper limits for a downgoing flu of IMMs with $g = g_D$, $2g_D$, $3g_D$ and for dyons (M+p , $g = g_D$) plotted vs β (for strong etching).

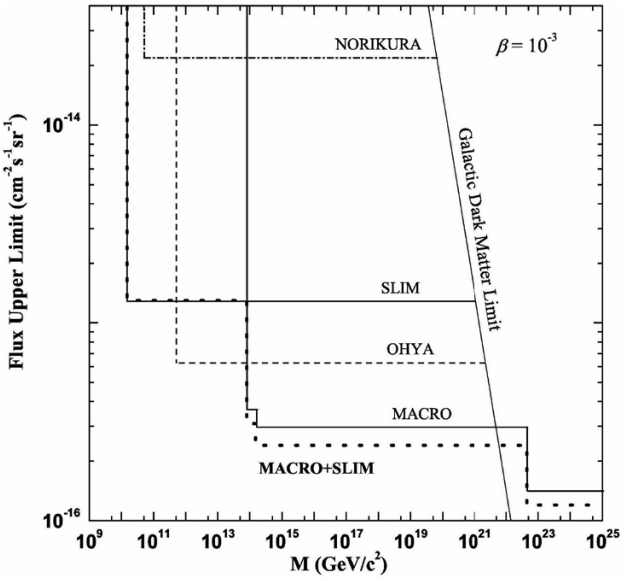

FIGURE 11. 90% C.L. flu upper limits versus mass for nuclearites with $\beta = 10^{-3}$ set by the SLIM and other NTD experiments. The combined MACRO+SLIM upper limit is also shown.

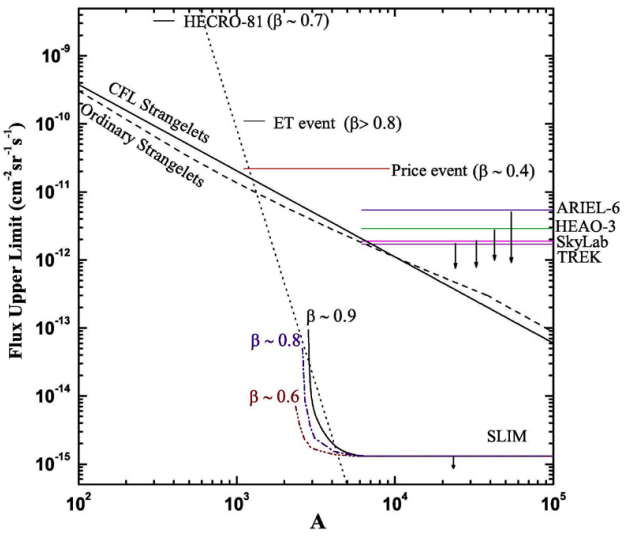

FIGURE 12. 90% C.L. flu upper limits versus baryon number A for light downgoing strangelets set by SLIM and experiments onboard balloons and satellites. The lines are the expected flu es based on different models: solid and dashed lines see [26] and refs. therein.

The main energy loss mechanism for low velocity nuclearites is via elastic or quasi-elastic collisions with the ambient atoms. The interaction of strangelets with matter is expected to be similar as for ordinary heavy ions but with a different (very small) charge to mass ratio [24,25]. They could be accelerated to relativistic velocities and be detected in CR39®NTDs [26].

In Fig. 9 is shown the REL versus β of (a) nuclearites and (b) strangelets of different masses in CR39®NTDs.

5.1. Status of the searches for massive MMs and SQM lumps in the CR

A search for GUT MMs was one of the primary goals of the MACRO experiment at LNGS (3700 m.w.e. depth). Different sub-detector systems (liquid scintillators, limited streamer tubes and NTDs) were used to have redundancy for the detection of MMs with different charges and velocities [27]. NTDs covered a surface of about 1300 m^2 for a total acceptance of $\sim$7100 m^2 sr to fast MMs. From a 10 years exposure a 90% CL flu upper limit was set at the level of 1.4×10^{-16} cm^{-2} s^{-1} sr^{-1}in the whole interesting β-range ($4\times10^{-5} < \beta < 0.1$); the MACRO result is the most stringent one for direct searches of such particles [12].

The SLIM experiment at the Chacaltaya (Bolivia) High Altitude Laboratory (5290 m a.s.l.) [28] was an array of 427 m^2 of CR39®and Makrofol detectors exposed for 4.2 years to cosmic rays. The detector was organized in modules of 24×24 cm^{2}area each consisting of stacks composed of 3 layers of CR39® interleaved with 3 layers of Makrofol DE® 2 layers of Lexan® and a 1 mm thick aluminum absorber to slow down nuclear recoils. Each stack was sealed in an aluminized plastic bag fille with 1 bar of dry air.

No candidates were found. The global 90% C.L. upper limits for the flu of downgoing IMMs with velocities $\beta > 4\times10^{-5}$ are shown in Fig. 10; for $\beta > 3\times10^{-2}$ the flu upper limit is $\sim 1.3\times10^{-15}$ cm^{-2} s^{-1} sr^{-1} [3].

In Fig. 11 are reported the limits obtained by various searches for galactic ($\beta \sim 10^{-3}$) nuclearites, performed with nuclear track detectors. Flux upper limits set for strangelets are shown in Fig. 12 [26].

6. Conclusion

The main features of NTDs is that they are easy to use detectors and have a very good (probably the best) charge resolution. NTDs offer outstanding possibilities in a wide range of applications, from nuclear physics to searches for exotic particles at accelerator facilities and in the cosmic radiation. The technique knew many improvements and important applications in the last decades; future progress in different areas can still be envisaged and discovered as well as the development of new detector materials.

Acknowledgments

We gratefully acknowledge the contribution from many colleagues, in particular S.Cecchini, D. Di Ferdinando, G. Giacomelli, M. Giorgini, E. Medinaceli, G. Sirri, V. Togo and C. Valieri.

i The bulk etching rate v_B is usually determined from the thickness of the removed material during etching.

1. R.L. Fleisher, P.B. Price, and R.M. Walker, *Nuclear Tracks in Solids*. (University of California Press, Berkeley, California 1975).
2. S. Balestra *et al.*, *Nucl. Instrum. Methods B* **254** (2007) 254.
3. S. Balestra *et al.*, *Eur. Phys. J. C* **55** (2008) 57.
4. V. Togo and I. Traoré, *Proceedings of the 24^{th}*, (1-5 Sept. 2008, Bologna, Italy).
5. P.A.M. Dirac, *Proc. R. Soc. London* **133** (1931) 60; Phys. Rev. **74** (1948) 817.
6. G. Giacomelli *et al.*, *Il Nuovo Cimento* **28** (1975) 212.
7. J. Derkaoui *et al.*, *Astropart. Phys.* **10** (1999) 339.
8. S. Cecchini *et al.*, *Nuovo Cimento* **109A** (1996) 1119.
9. G. Giacomelli and L. Patrizii, *Magnetic monopole searches* (2005); hep-ex/0506014; (2003) hep-ex/0302011
10. G.R. Kalbfleisc *et al.*, *Phys. Rev. Lett.* **85** (2000) 5292; hep-ex/0005005.
11. K.A. Milton *et al.*, *New limits on the production of Magnetic Monopoles at Fermilab* (2000); hep-ex/0009003.
12. M. Ambrosio *et al.*, *Eur. Phys. J. C* **25** (2002) 511.
13. K. Kinoshita *et al.*, *Phys. Rev. D* **46** (1992) R881.
14. M. Bertani *et al.*, *Europhys. Lett.* 12 (1990) 613.
15. B. Abbott *et al.*, *Phys. Rev. Lett.* **81** (1998) 524; M. Acciarri *et al.*, *Phys. Lett. B* **345** (1995) 609.
16. J.L. Pinfold, *Proceedings of the 24^{th}* (ICNTS, 1-5 Sept. 2008, Bologna, Italy).
17. H. Dekhissi *et al.*, *Nucl. Phys. A* **662** (2000) 207; S. Cecchini *et al.*, *Nucl. Phys. A* **707** (2002) 513.
18. S. Cecchini *et al.*, *Nucl. Phys. A* **807** (2008) 206.
19. G. Giacomelli, *Riv. Nuovo Cimento* **12** (1984) 1.
20. J. Preskill, *Ann. Rev. Nucl. Part. Sci.* **34** (1984) 461.
21. G. Lazarides, C. Panagiotakopoulos, and Q. Shafi *Phys. Rev. Lett.* **58** (1987) 1707; T.W. Kephart and Q. Shafi *Phys. Lett. B* **520** (2001) 313.
22. A. De Rujula and S.L. Glashow, *Nature* **312** (1984) 734.
23. E. Witten, *Phys. Rev. D* **30** (1986) 272.
24. H. Heiselberg, *Phys. Rev. D* **48** (1993) 1418.
25. J. Madsen, *Phys. Rev. Lett.* **87** (2001) 172003.
26. S. Cecchini *et al.*, *Eur. Phys. J. C* **57** (2008) 525.
27. M. Ambrosio *et al.*, *Nucl. Instrum. Methods* **324** (1993) 337; *Nucl. Instrum. Methods* **486** (2002) 663.
28. S. Cecchini *et al.*, *Nuovo Cimento C* **24** (2001) 639.